Journal of Molecular Structure 1347 (2025) 143307

Contents lists available at ScienceDirect

Journal of Molecular Structure

journal homepage: www.elsevier.com/locate/molstr

Compression rate-driven amorphization in pyrrole: static vs. dynamic pressure conditions

Qingqing Yang [a], Chaosheng Yuan [a,*], Yongfu Liang [a], Xiang Zhu [a], Zheng Wang [a], Kai Shi [a], Xuerui Cheng [a], Lei Su [b,c,*]

[a] Electronic information school, Zhengzhou University of Light Industry, Zhengzhou, Henan, 450002, China
[b] Center for High Pressure Science and Technology Advanced Research, Beijing 100093, China
[c] Shanghai Advanced Research in Physical Sciences, Shanghai 201203, China

ARTICLE INFO

Keywords:
Dynamic compression
Amorphization, pyrrole
Phase transition

ABSTRACT

The phase transition of pyrrole was studied under static pressure and dynamic pressure by in situ Raman spectroscopy. Under static compression, pyrrole underwent three phase transitions: a liquid-to-crystal (phase I) transition at 1.15 GPa, followed by transformation into phase II at 7.45 GPa and the start of amorphous phase transition at 16 GPa. Under dynamic compression, pyrrole was compressed into an amorphous phase as the pressure increased from 0.71 GPa to 5.02 GPa, 8.07 GPa, 10.30 GPa, 11.30 GPa and 12.84 GPa within 5 ms, respectively. Rapid compression rate and high pressure provide a greater degree of disorder in amorphous pyrrole by fitting the partial Raman peak linewidth with pressure. During the pressure relief process, the amorphous pyrrole crystallized and transformed into phase II at 3.20 GPa and then reverted to its initial liquid state at around 0.55 GPa. The phase behaviors can be attributed to different solidification mechanisms of liquid pyrrole induced by different compression rates under the two compression conditions.

1. Introduction

Over the past few decades, research on aromatic compounds under extreme conditions has received extensive attention [1]. This subject has potential applications in fields such as nanomaterials, as the unique phase transition mechanisms of aromatic compounds offer ideal models for high-pressure physical chemistry research [2]. High-pressure approaches may be applied by drastically lowering the molecular spacing and modifying the electron cloud distribution and produce unusual bond rearrangements in aromatic compounds [3]. Therefore, pressure offers a useful method for investigating the microscopic processes behind intricate phenomena like pressure-induced amorphization and polymerization [4]. Taking benzene-based compounds as an example, Li's research group precisely determined the critical reaction pressure (2.0×10^6 atm) of the benzene-hexafluorobenzene eutectic system [5]. Their work proposed a reaction mechanism dominated by the Diels-Alder cycloaddition reaction, thereby unveiling a novel pathway for high pressure polymerization processes.

Pyrrole (C_4H_5N), a nitrogen-containing five-membered heterocyclic compound, derives its unique chemical and physical properties from an aromatic system and lone pair electrons within its molecular structure [6]. This structure underpins pyrrole's significant utility in diverse fields, including polymer materials, biomedicine, and optoelectronic devices [7]. Notably, pyrrole-derived polymers exhibit excellent optoelectronic characteristics, enabling their widespread application in advanced devices such as organic photovoltaics (OPV) and organic field-effect transistors (OFET) [8]. Recent advances in high-pressure experimental techniques (e.g., diamond anvil cell, in-situ spectroscopy) and computational methods have facilitated substantial progress in understanding pyrrole's high-pressure behavior. Optoelectronic characteristics, reaction routes, structural phase transitions, and the creation of functional materials with pressure as a tuning parameter are important areas of progress [9–12]. These developments provide new opportunities for elucidating the structure-property relationships of heterocyclic molecules under extreme conditions.

Pressure is a pivotal external parameter for modulating pyrrole-based systems. For instance, pressure drives a dimensionality crossover in polypyrrole conduction, as evidenced by conductivity measurements: from three-dimensional variable-range hopping at low pressure toward one-dimensional intrachain dominance driven by

* Corresponding authors.
E-mail addresses: zzyuancs@zzuli.edu.cn (C. Yuan), lei.su@sharps.ac.cn (L. Su).

https://doi.org/10.1016/j.molstruc.2025.143307
Received 24 April 2025; Received in revised form 2 July 2025; Accepted 13 July 2025
Available online 13 July 2025
0022-2860/© 2025 Elsevier B.V. All rights are reserved, including those for text and data mining, AI training, and similar technologies.

enhanced π-π stacking [13]. Pressure also significantly boosts pyrrole oligomerization efficiency in high-pressure plasma environments, confirming its regulatory role in synthesis pathways [14]. These studies demonstrate pressure's ability to reshape pyrrole's electrical, optical, and chemical properties through altered intermolecular interactions. Crucially, pressure directly induces key phase transitions in pyrrole. While liquid under ambient conditions, pyrrole solidifies below 103 K into an orthorhombic phase (*Pnma*) [15,16]. Room-temperature compression triggers sequential phase changes: (1) a liquid-solid transition at ~0.6 GPa via π-stacking reorientation; (2) a solid-solid transition (*Pnma* to $P2_1/c$) with ~40 % volume collapse at ~6.2 GPa; and (3) the onset of a crystalline-amorphous transition at ~14.3 GPa [17].

High pressure serves as a powerful tool for molecular structure regulation, enabling the synthesis of crystals that are otherwise challenging to grow under environmental conditions [18,19]. Recently, the effect of compression rate on the crystallization kinetics was studied by some groups. For example, hexagonal ice transforms to thermodynamically stable phase ice II at a rate of 0.01 GPa/min, while metastable ice III transforms at a rate of 1 GPa/min [20]. Similar phenomena have also seen in investigations of L-serine, 2-fluorophenylacetylene, 3-nitrophenylacetylene, and pyridine [21–24]. In addition, for some irreversible processes, special phases are often generated during the decompression. Chu et al. [25] reported the transformation of Choline chloride/Ethylene glycol deep eutectic solvent from an amorphous phase to a crystalline phase at a slow pressure release from 5.0 GPa to 1.8 GPa. Wang et al. [26] reported the transformation of amorphous 4-methylpyridine into new crystals I' at 2.40 GPa during pressure release.

In this work, in situ high-pressure Raman spectroscopy was used to study the phase transition of pyrrole under static and dynamic compression. The static compression results show that the samples experienced a liquid-solid phase transition and a solid-solid phase transition at around 1.15 GPa and 2.20 GPa, respectively, and then began to undergo amorphization transformation above 16 GPa. In the dynamic compression experiment, pyrrole liquid underwent a transformation into an amorphous phase upon fast compression rate. It is worth noting that the pressure relief process was studied in detail and a transient crystalline phase was observed during the decompression.

2. Experimental methods

A Merrill-Bassett type four-screw diamond anvil cell (DAC) with two diamonds of 300 μm in size was used for all experiments. To serve as the sample chamber, a hole with a diameter of 80 μm was drilled at the center of a 300 μm thick T301 gasket, which had been pre-indented to a depth of 60 μm. The empty hole in the DAC gasket was filled with 99 wt % pure pyrrole liquid, which was purchased from Shanghai Aladdin Pharmaceutical Co., Ltd.. A little ruby chip was also placed within the hole. Subsequently, the gasket was sealed with the opposite anvil. The chamber pressure was calibrated by using the ruby *R1* fluorescence line [27].

Two experiments (static and dynamic compression) were conducted when pyrrole was subjected to extreme conditions. A standard four-screw diamond anvil cell (DAC) was used for static compression experiments, in which the sample was steadied and gradually compressed before Raman spectra were gathered. Dynamic compression experiments were conducted on the d-DAC, which is constituted by a metal frame, a piezoelectric (PE) actuator, a control system, and a standard DAC. The PE actuator (Harbin Core Tomorrow Science & Technology Co., Ltd.) was assembled on the top of the metal frame. A conventional DAC was fixed at the bottom of the metal frame by a steel plate and a static load screw. The pressure control system can be configured to provide an output voltage within the range of 0 to 120 V, and this device can achieve a pressure jump within 5 ms. The load on the sample was provided by the PE actuator and was driven by a variable electronic signal from a function generator (see Ref. [28] for a detailed description of d-DAC).

Raman spectroscopy experiment was carried out using a Renishaw inVia Raman microscope (Renishaw, United Kingdom) with a wavelength excitation of 532 nm. Raman spectra were collected in a backscattering geometry with a 2400 g/mm holographic grating, and the slit width was selected as 65 μm, which corresponded to a resolution of approximately 0.5 cm^{-1}. The sample image was collected through an achromatic lens of an optical microscope and then focused onto a charge-coupled device (CCD) detector for visual monitoring during experiments. The obtained Raman spectra were fitted with a mixed Gaussian-Lorentzian function using WIRE 3.3 software (Renishaw, United Kingdom) to analyze the spectral data.

3. Results and discussion

3.1. Static compression

The Raman spectra of the pyrrole in the region of 50–3500 cm^{-1} under static compression at room temperature are shown in Fig. 1. The lattice vibration region is located below 200 cm^{-1} and the 500–1350 cm^{-1} range is mainly composed of C—H and N—H bending vibration regions. The Raman band at about 1381 cm^{-1} could be assigned to the ring frame C = C vibration and C—H bend, as well as the band at 1471 cm^{-1} is contributed to the ring frame C = C vibration and N—H bend. In addition, the Raman bands above 3000 cm^{-1} are corresponded to the stretching vibration of C—H and N—H [17]. The list of observed crystal vibrational modes along with their frequencies and assignments is given in Table I.

As shown in Fig. 1, most of the Raman characteristic peaks shift to the higher wavenumbers with increasing pressure, which is explained by the contraction of adjacent molecules or atom distances [29]. At 1.15 GPa, four Raman peaks emerged at 94, 130, 158, and 175 cm^{-1} in the lattice vibration region and two weak peaks at 3109 cm^{-1} and 3140 cm^{-1} split into three sharp peaks at 3114, 3123, and 3142 cm^{-1}. Sharper profiles with increased signal clarity are seen in the Raman peaks at 1148 cm^{-1}, 1381 cm^{-1}, and 1470 cm^{-1}. These features indicate that pyrrole underwent a liquid-to-crystal (phase I) transition at 1.15 GPa. As the pressure increases to 2.20 GPa, two new Raman peaks emerge at 608 and 665 cm^{-1} in the region of the C—H and N—H bending vibrations. As well, a new lattice vibrational mode appears at 126 cm^{-1} and two sharp peaks emerge at 3346 and 3362 cm^{-1}. It means that pyrrole underwent a solid-solid (phase I to II) phase transition at 2.20 GPa. Further compression to 7.45 GPa, another new lattice vibrational mode split from the original peak emerges at 209 cm^{-1}, and the Raman mode at 892 cm^{-1} can be clearly discerned. According to Li's research [17], pyrrole undergoes the continuous I-to-II phase transition that starts at 2.60 GPa and ends at 6.50 GPa. From this, it can be inferred that the phase transition takes place at 2.20 GPa and then completes at 7.45 GPa in this work. Tables SI-SII display the atomic coordinates of pyrrole phases I and II. When the pressure continues to increase beyond 16 GPa, the Raman peak gradually broadens, and meanwhile the peak intensity gradually decreases, which means that pyrrole gradually transitions from phase II to amorphous state above 16 GPa.

Fig. 2 shows the pressure dependence of Raman shifts and the full width at half maximum (FWHM) of pyrrole, along with images of pyrrole under different pressures. Except for 3354 and 3368 cm^{-1}, the primary distinctive peaks moved to a high wavenumber with increasing pressure, as seen in Fig. 2(a-d). Additionally, the Raman shifts show a discontinuity as a function of pressure around roughly 2.20–7.45 GPa. Moreover, the FWHM of the ring frame C = C vibration at 1467 cm^{-1}, the C—H and N—H in-plane rocking at 1143 cm^{-1}, and the C—H out-of-plane wiggling at 576 cm^{-1} showed abrupt changes at pressures of 1.15, 2.20, and 7.45 GPa in Fig. 2(e). These results indicate that pyrrole undergoes two phase transition processes at 1.15 GPa and 2.20 GPa under static high pressure, which is consistent with the analysis of the Raman spectra. Specially, the obvious discontinuous range from 2.20 to

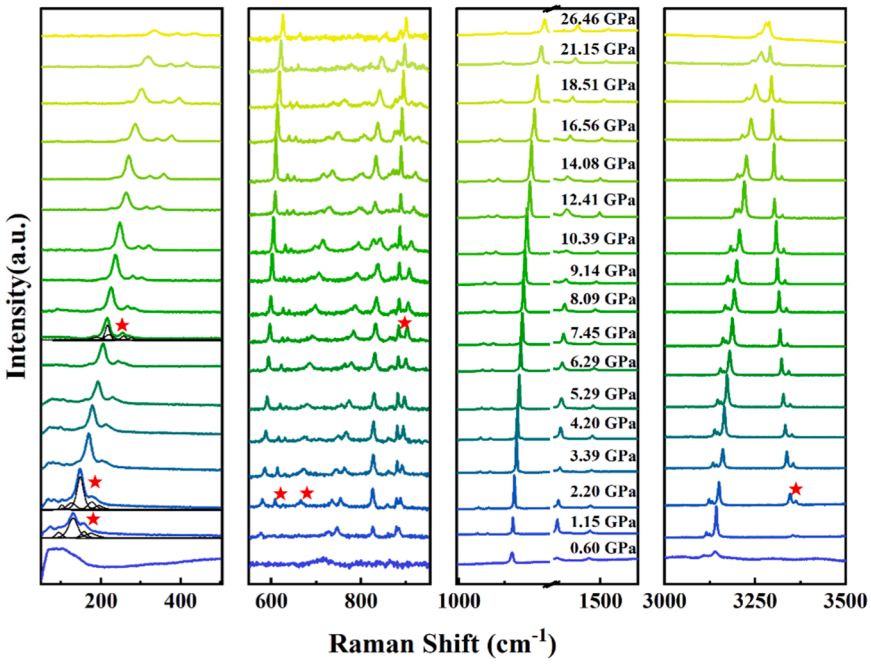

Fig. 1. Raman spectra of pyrrole under different static pressures.

Table I
Assignments of the major bands in the Raman spectrum of pyrrole.

Liquid (cm^{-1})	Crystal (cm^{-1})	Ref Exp (cm^{-1}) [17]	Vibrational assignment
–	74	78	lattice vibration modes
–	94	99	
–	130	130	
–	158	141	
–	175	157	
–	576	578	C − H out-of-plane wag
–	601	604	C − H and N − H out-of-plane wag
–	727	724	C − H out-of-plane wag
–	826	829	C − H, N − H in-plane bend
–	878	862	C − H in-plane bend
–	882	868	*C − H* in-plane bend
–	884	881	C − H in-plane bend
–	1045	1047	C − H in-plane rocking
–	1051	1053	C − H and N − H in-plane rocking
–	1078	1079	C − H in-plane rocking
1143	1148	1139	ring breathing vibration and C − H in-plane bend
–	1162	1147	C − H and N − H in-plane rocking
–	–	1248	C − H and N − H in-plane rocking
1380	1381	1380	ring frame C = C vibration and C − H bend
1467	1471	1471	ring frame C = C vibration and N − H bend
3105	3114	3108	C − H stretch
–	3122	3117	C − H stretch
3136	3142	3136	C − H stretch
–	3354	3359	N − H stretch
–	3369	3374	N − H stretch

7.45 GPa show the coexistence state of phase I and phase II. In addition, it is also demonstrated that pyrrole progressively changes to an amorphous state at 16 GPa, since the FWHM of 578, 1143, and 1467 cm^{-1} similarly appears as an inflection point around 16.56 GPa.

In addition, Fig. 2(f) shows the in-situ micrograph of the pyrrole under different pressures. The sample was totally transparent, and the ruby chips could be clearly observed at 0.6 GPa. And then, at around 1.15 GPa, crystal formation was seen in the sample cell. This clearly illustrates the pyrrole's pressure-induced crystallization behavior, which was in line with the previously described Raman findings. As the pressure further increased to 2.20 GPa, the boundaries of the crystal became more pronounced and the layers became more distinct compared to crystals under 1.15 GPa, which implies a higher-density phase of pyrrole. When the pressure exceeds 15.84 GPa, the boundaries of the crystals become blurred, and the hierarchical sense of the crystal shapes gradually weakens. These observations further support the amorphization of the pyrrole crystals as previously suggested by Raman spectroscopy.

3.2. *Dynamic compression*

Under dynamic compression, the pyrrole sample was compressed slowly to 0.71 GPa and then compressed rapidly to higher pressure. Fig. 3 shows the Raman spectrum of pyrrole compressed rapidly from 0.71 GPa to 5.12, 8.02, 10.30, and 12.84 GPa within 5 ms, respectively. As seen in Fig. 3, in comparison to the sample at 0.71 GPa, the major Raman peaks shift to higher wavenumbers and exhibit significant broadening as the pressure increases rapidly from 0.71 GPa to 5.12 GPa. The Raman spectrum between 50–300 cm^{-1} features a broad peak centered at 191 cm^{-1}, with no observable splitting of lattice vibrational modes. And there was no sign of splitting in the Raman peaks related to the stretching vibrations of C—H and N—H within the wavenumber range exceeding 3000 cm^{-1}. In addition, the sample cell exhibited high optical transparency, and no well-defined interfaces or geometric features are discernible (see the inset photograph in Fig. 3). These results indicate that the pyrrole liquid was solidified as an amorphous phase during the dynamic compression process. Consistent findings were similarly noted in Samples DP-8.02 GPa, DP-10.30 GPa, and DP-12.84 GPa. Despite variations in pressure magnitude and compression rates, the pressure-induced solidification of liquid pyrrole resulted in reproducibly consistent microstructural states. Notably, Raman spectroscopy revealed broadened peaks with no resolvable peak splitting, and no distinct crystalline phases were discernible within the sample cell (see the inset photograph in Fig. 3). Therefore, it seems from the experimental data that the liquid pyrrole also solidified as an amorphous phase from 0.71 GPa to 8.02 GPa, 10.30 GPa, and 12.84 GPa, respectively, during the rapid compression. Furthermore, we used spectral fitting to examine the full width at half maximum (FWHM) of Raman peaks at 1146 cm^{-1} and 3141 cm^{-1} for each of the four samples. The results indicated that for samples DP-5.12 GPa to DP-12.84 GPa, the FWHM

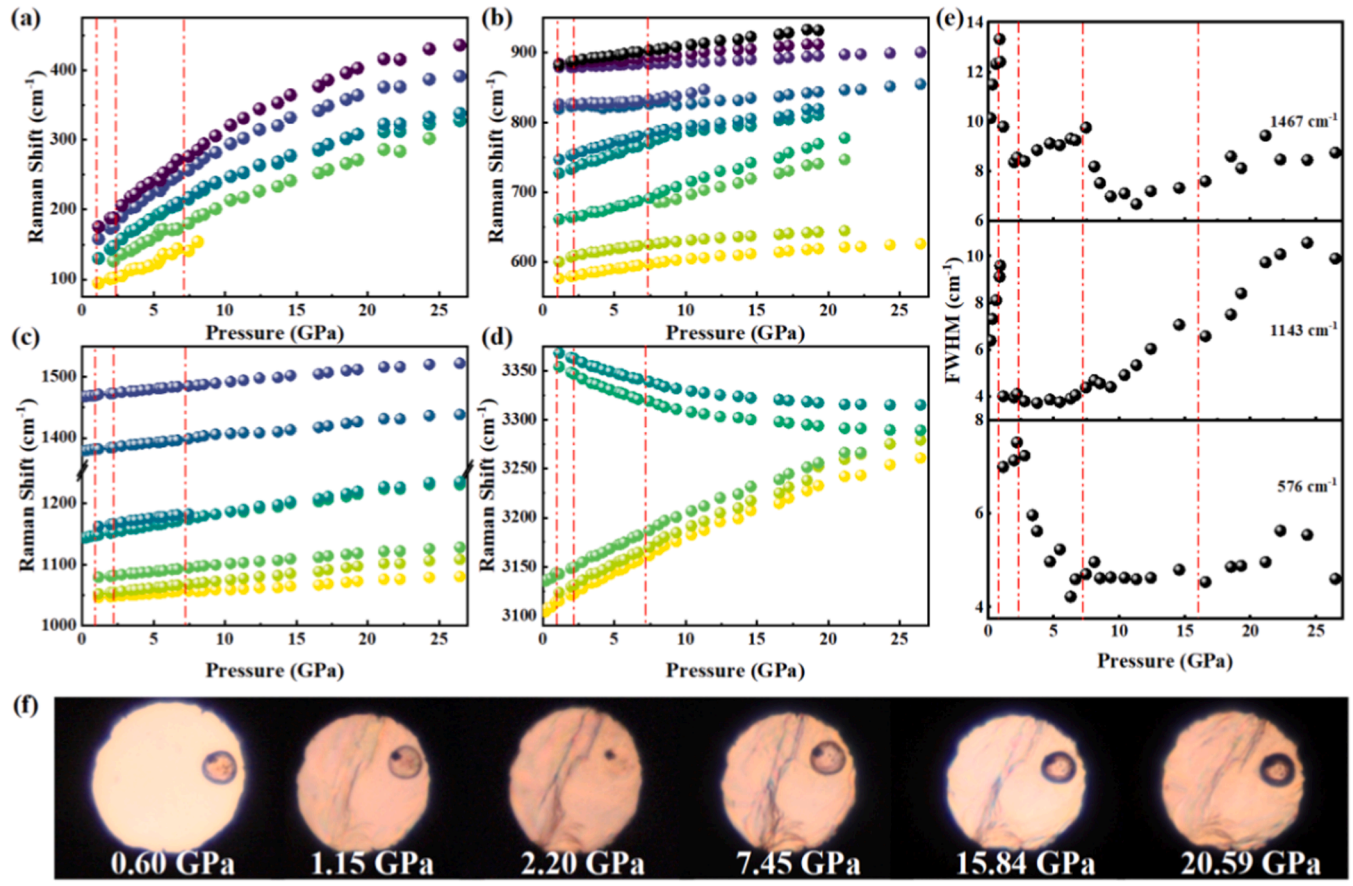

Fig. 2. (a) (b) (c) and (d) Relationship among pressure, Raman shifts, and some vibrational modes, (e) relationship between pressure and the FWHM of the vibrational modes of pyrrole, (f) Photographs of the sample under different pressure.

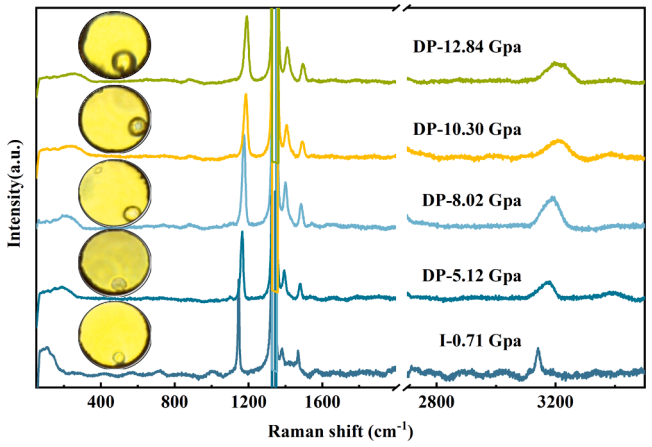

Fig. 3. Raman spectrum of pyrrole compressed rapidly from 0.71 GPa to 5.12, 10.30, 8.02, and 12.84 GPa, respectively. The inset shows photograph of the sample at the corresponding pressure. "DP-" represents dynamic compression; "I-" represents initial pressure.

values of the peaks at 1165 cm^{-1} and 3144 cm^{-1} were 16.22 cm^{-1}, 19.98 cm^{-1}, 23.22 cm^{-1}, 24.88 cm^{-1}, and 56.27 cm^{-1}, 66.24 cm^{-1}, 83.64 cm^{-1}, 85.65 cm^{-1}, respectively. These findings unequivocally show that the structural disorder in the solidified amorphous pyrrole increases dramatically with increasing compression rate and applied pressure. This observation clearly implies that the faster compression rates and higher pressures lead to the formation of more disordered solid states in such aromatic materials, which might be associated with the degree of undercooling achieved during the rapid compression process [20].

Intriguingly, when the pyrrole was compressed rapidly from 0.71 GPa to 11.30 GPa in 5 ms, the coexistence of the crystalline and amorphous phases was discovered in the pyrrole sample cavity. Fig. 4 shows the Raman spectra of pyrrole DP-11.30 GPa at the different regions and the photograph of sample cell. A close examination of Fig. 4(a) shows that, besides the ruby sphere, a clear border roughly separates the sample cell into two clear areas. In particularly, **region 1** exhibits a distinct shape with surface striations that interlace. The corresponding Raman spectrum demonstrates the sharpening of the Raman peaks together with the appearance of many additional peaks. For example,

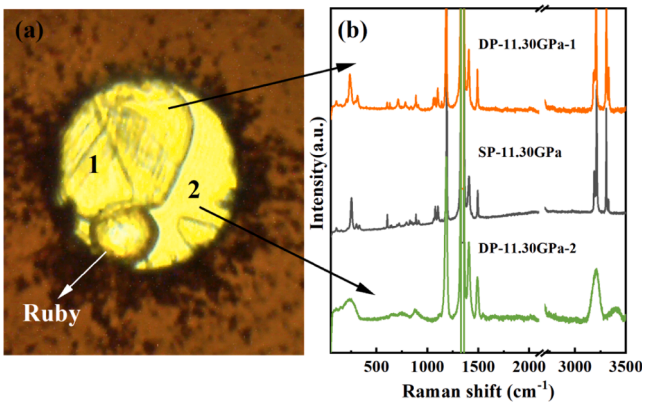

Fig. 4. (a) Photograph of the sample at DP-11.30 GPa. (b) Raman spectrum of pyrrole compressed rapidly from 0.71 GPa to 11.30 GPa in 5 ms. "SP-" represents static compression.

five distinct lattice vibration peaks are observed within 50–300 cm^{-1}, while five C—H vibrations emerge in the 3000 and 3200 cm^{-1} region. The solid sample in **region 1** is in the crystalline phase II of pyrrole, according to these results, which are in keeping with those of the sample at the same static pressure. **Region 2**, on the other hand, has no discernible texture or structural characteristics and shows excellent optical transparency. In contrast to liquid pyrrole, the associated Raman spectrum shows expanded typical peaks without the appearance of additional spectral characteristics. These findings point to the solid sample in **region 2** being the amorphous phase of pyrrole. The co-existence phenomenon can potentially be ascribed to the local shear force arising from the pressure gradient within the cavity during the initial stage of rapid compression. For the overpressurized pyrrole liquid, the local shear field could restrict molecular rotation and diffusion, lower the nucleation energy barrier and accelerate the formation of long-range ordered lattices. And then, intermolecular interactions improve dramatically and molecular viscosity rises noticeably as pressure increases rapidly. The crystallization process is hampered by the combined impact of limiting molecular diffusion and mobility.

Furthermore, the stability of the amorphous pyrrole formed under dynamic pressure was investigated using Raman spectroscopy throughout the gradual pressure release process. Fig. 5 shows the decompression Raman spectra of pyrrole DP-10.30 GPa and the photograph during the pressure release process. As shown in Fig. 5(a), all of the Raman peaks move to the lower wavenumber when the pressure is progressively decreased to 3.25 GPa; neither the new peaks nor the old peaks emerge or vanish, suggesting that the amorphous phase of pyrrole remains unchanged throughout this process.

Remarkably, a few crystals began to form near the cavity's border when the pressure was further lowered to 3.17 GPa, as seen in Fig. 5(b). These crystals filled the space with fine-grained crystals after two minutes of sustaining the pressure, and they grew to fill a sizable amount of the chamber in just one minute. After pyrrole completely crystallized, the pressure in the sample cavity dropped to 2.84 GPa. This was because the atoms were rearranged in an orderly fashion, which removed the excess free volume that was present in the amorphous form. Correspondingly, at a pressure of 2.84 GPa, the Raman spectrum reveals the emergence of Raman peaks at 165, 826, 3338, and 3354 cm^{-1}, which are characteristic of the crystalline phase. Moreover, the C—H vibration centered at 3160 cm^{-1} splits into three distinct peaks at 3130, 3140, and 3157 cm^{-1}. Given the similarity of these Raman peaks to those of pyrrole's phase II under static pressure, it's clear that phase II is the crystalline phase emerging during pressure release. Upon further depressurization to 0.55 GPa, all Raman peaks exhibited minor broadening, with no spectral features detected in the lattice vibrational region. Moreover, peaks at 500–1100 cm^{-1} and ~3300 cm^{-1} vanished completely. At 0.55 GPa, the pyrrole sample returned to its initial liquid condition, as evidenced by the pressure-release Raman spectra that nearly matched the original one. Fig. 5(c) illustrates the melting transition of crystalline pyrrole at 0.55 GPa, which is consistent with the Raman results.

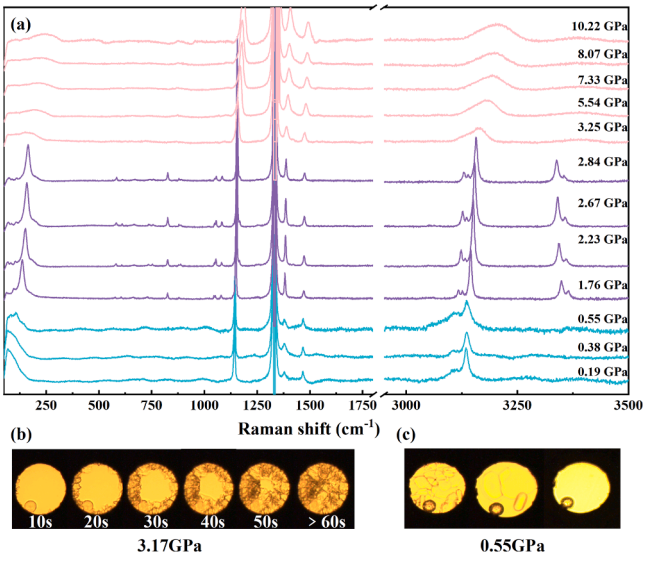

Fig. 5. (a) Raman spectrum of pyrrole decompressed from dynamic compression at 10.30 GPa, (b) Photograph of pyrrole crystallization process by decompression at 3.17 GPa. (c) Photograph of the crystal melting process of pyrrole at 0.55 GPa.

Additionally, it seems that the phase transition behavior of amorphous pyrrole during the depressurization process is repeatable. Fig. 6 presents the Raman spectra of pyrrole DP-5.12 GPa, DP-8.07 GPa, DP-11.30 GPa, and DP-12.84 GPa released to around 3.30 GPa. All samples showed crystallization when the pressure was lowered to around 3.10 GPa, and the locations and forms of the Raman peaks closely matched those of SP-3.30 GPa under static pressure. When depressurized further to 0.6 GPa, these crystals melted back into liquid pyrrole over time. As mentioned above, static compression induces a continuous phase I→II transition (2.20–7.45 GPa), with phase II stable up to 16 GPa. However, phase II appears during amorphous phase decompression (0.55–3.20 GPa) under dynamic compression. Using $dG=VdP$ for decompression ($dP<0 \rightarrow dG<0$), the II→I transition is thermodynamically spontaneous. Therefore, the stability of phase II stems from kinetically trapped metastability, highlighting dynamic kinetics in non-equilibrium phase behavior. By recrystallizing the amorphous phase under decompression, Liu *et al.* were able to achieve the metastable state of certain materials (eg. chalcohalide inorganic compound and hybrid perovskites) [30,31]. They noted that the decompression process may be seen as reverse loading, in which modulus softening of the soft sublattice (G↓) significantly lengthens the relaxation period (τ↑). The growing duration of τ is made worse by the low modulus of pyrrole, a tiny organic molecule. When the decompression rate (dP/dt) significantly exceeds the structural recovery rate of the soft sublattice, kinetic "structural freezing" prevents full reversible reconstruction of the lattice, even in thermodynamically spontaneous conditions ($dG<0$). This would lead to the formation of the kinetically metastable phase II.

3.3. Discussion

As mentioned above, liquid pyrrole undergoes a liquid-solid phase transition at 1.15 GPa under static compression, followed by a solid-solid phase transition at 7.45 GPa, and gradually amorphizes above 16

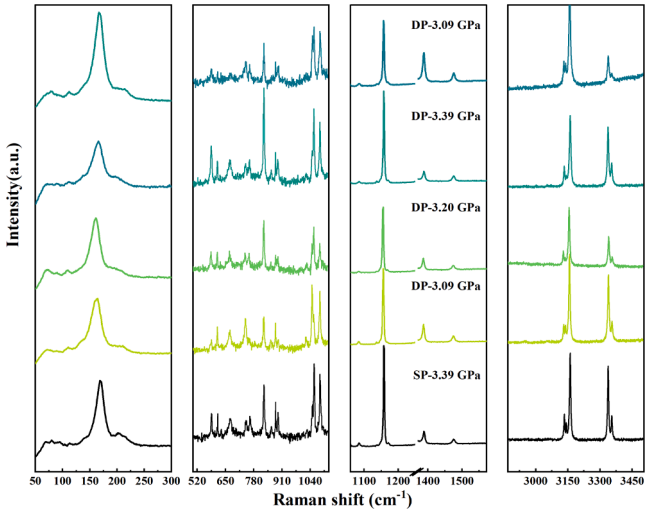

Fig. 6. Raman spectra of pyrrole released from DP-5.12 GPa, DP-8.07 GPa, DP-11.30 GPa, and DP-12.84 GPa to 3.09, 3.39, 3.20, and 3.09 GPa, respectively.

GPa. Conversely, under dynamic compression, pyrrole transforms directly into the amorphous phase as the pressure increases rapidly from 0.71 GPa to 5.12, 8.02, 10.30, and 12.84 GPa within 5 ms, respectively. This discrepancy may be attributed to differing solidification mechanisms of liquid pyrrole under the two compression regimes.

Under static compression, the compression rate is modest and the pressure amplitude is minimal. In general, this process is thought to be "quasi-isothermal". The intermolecular contact gets stronger as the intermolecular distance steadily shrinks during the progressive compression of pyrrole. The Clapeyron equation ($\Delta G = V\Delta P$) predicts that the compression of molecular space ($\Delta V < 0$) greatly increases the strength and directionality of N—H···π hydrogen bonds. This forces pyrrole molecules to take on ordered configurations, including cyclic tetramers supported by cooperative N—H···π interactions. These configurations are energetically advantageous because of the optimized π-π stacking geometry and decreased intermolecular repulsion, as a result, pyrrole liquid solidified as crystal phase I under static pressure of 1.15 GPa.

Under dynamic compression, both the compression rate and the pressure amplitude are relatively high, which prevents the system from exchanging energy with the external environment quickly. Therefore, this process is generally regarded as a "quasi-adiabatic" process [32]. In this study, the compression rate reached 1024, 1614, 2060, 2260, and 2568 GPa/s, respectively, as the pyrrole liquid was compressed quickly from 0.71 to 5.12, 10.30, 8.02, and 12.84 GPa. Pyrrole's intermolecular distance shrinks and the π-π connection is strengthened during compression, which limits molecular mobility. Rapidly declining free volume prevents molecules from diffusing and rearranging over extended distances. Poisson's equation (PV^{γ}=C, γ=Cp/Cv, the adiabatic index; *C* is constant) indicates that multi-step compression with small pressure amplitudes maintains the pyrrole molecules in near-thermodynamic equilibrium via quasi-static compression, approximating an adiabatic reversible process with entropy conservation, favoring stable phase formation through gradual structural adjustment. In contrast, during single-step dynamic compression with large amplitudes, the adiabatic process causes significant and rapid deviations from thermodynamic equilibrium. The high strain rate and instantaneous energy input in dynamic compression would lead to non-equilibrium thermodynamic state, where pyrrole molecules may lack sufficient time for structural relaxation to reach the lowest free energy state. Consequently, this kinetic constraint promotes the formation of amorphous pyrrole with higher free energy [33,34], which are kinetically trapped due to the inability to achieve thermodynamic equilibrium under rapid compression conditions.

4. Conclusion

In summary, the phase transitions of pyrrole under static and dynamic compression were measured by Raman spectroscopy. Under static compression, pyrrole underwent three phase transitions: a liquid-to-crystal (phase I) transition at 1.15 GPa, followed by the transformation into phase II at 7.45 GPa and the start of amorphous phase transition at 16 GPa. Furthermore, the phase transition behavior of pyrrole under dynamic compression was examined with a d-DAC. As the pressure jumped from 0.71 GPa to 5.02 GPa, 8.07 GPa, 10.30 GPa, and 12.84 GPa within 5 ms, respectively, liquid pyrrole solidified into an amorphous phase. As the compression rate and pressure amplitude increase, the degree of amorphization of pyrrole becomes more pronounced. According to conjecture, dynamic compression provides a fast non-equilibrium compression path, where pyrrole molecules rapidly freeze and transform into the amorphous phase during rapid compression. While the pressure was rapidly compressed from about 0.70 GPa to 11.30 GPa, the coexistence of the amorphous and crystalline phases in pyrrole was observed. This phenomenon is thought to be caused by the shear stress that occurs inside the sample during fast compression. Interestingly, the crystalline phase II of pyrrole was observed during the decompression of its amorphous phase. This phase stayed stable in the range of 0.55–3.20 GPa before returning to its original liquid condition. This novel phase transition behavior under dynamic compression can be attributed to the effect of compression rate on the crystallization kinetics of pyrrole.

CRediT authorship contribution statement

Qingqing Yang: Writing – original draft, Methodology, Data curation. **Chaosheng Yuan:** Writing – review & editing, Writing – original draft, Methodology, Investigation, Funding acquisition, Data curation, Conceptualization. **Yongfu Liang:** Software, Methodology, Funding acquisition. **Xiang Zhu:** Methodology, Data curation. **Zheng Wang:** Validation, Supervision. **Kai Shi:** Validation, Project administration. **Xuerui Cheng:** Project administration, Data curation. **Lei Su:** Methodology, Investigation, Conceptualization.

Declaration of competing interest

We declare that we have no financial and personal relationships with other people or organizations that can inappropriately influence our work, there is no professional or other personal interest of any nature or kind in any product, service and/or company that could be construed as influencing the position presented in, or the review of, the manuscript entitled.

Acknowledgments

This work is supported by the National Science Foundation of China (No.21503194; No. 12104415); the Scientific Research Key Project Foundation of Henan Province (No.242102230109; No.232102230151; No.252102241031); Natural Science Foundation of Henan Province (No.252300420354).

Supplementary materials

Supplementary material associated with this article can be found, in the online version, at doi:10.1016/j.molstruc.2025.143307.

Data availability

Data will be made available on request.

References

[1] S. Block, C.E. Weir, G.J. Piermari, Polymorphism in benzene, naphthalene, and anthracene at high pressure, Science 169 (1970) 586–587.
[2] S. Huss, S. Wu, B. Chen, et al., Scalable synthesis of crystalline one-dimensional carbon nanothreads through modest-pressure polymerization of furan, ACS Nano 15 (3) (2021) 4134–4143.
[3] L. Lei, L.L. Zhang, Recent advance in high-pressure solid-state metathesis reactions, Matter. Radiat.. Extremes 3 (3) (2018) 95–103.
[4] S.M. Sharma, S.K. Sikka, Pressure induced amorphization of materials, Prog. Mater. Sci. 40 (1996) 1–77.
[5] Y.J. Wang, X. Dong, X.Y. Tang, et al., Pressure-induced diels-alder reactions in C_6H_6-C_6F_6 cocrystal towards graphane structure, Angew. Chem. Int. Ed. 58 (2019) 1468.
[6] T. Shi, G.F. Yin, X.D. Wang, et al., Recent advances in the syntheses of pyrroles, Green Synth. Catal. 4 (1) (2023) 20–34.
[7] V.F. Ferreira, M.C.B.V. de Souza, A.C. Cunha, et al., Recent advnces In the synthesis of Pyrroles, Org. Prep. Proced. Int. 33 (5) (2001) 411–454.
[8] C. Bulumulla, R. Gunawardhana, P.L. Gamage, et al., Pyrrole-containing semiconducting materials: synthesis and applications in organic photovoltaics and organic field-effect transistors, ACS Appl. Mater. Interfaces 12 (29) (2020) 32209–32232.
[9] Q. Li, Z.W. Chen, M.Z. Li, et al., Pressure-engineered photoluminescence tuning in zero-dimensional lead bromide trimer clusters, Angew. Chem. Int. Ed. 60 (2021) 2583.
[10] I.OrgzallH J.Mikat, D. Hochheimer, Raman spectroscopy of conducting polypyrrole under high pressure, Phys. Rev. B 65 (2002) 174202.
[11] L. Zhai, X.F. Zhou, R.F. Liu, et al., A theoretical study of pyrolysis mechanisms of pyrrole, J. Phys. Chem. A 103 (20) (1999) 3917–3922.

[12] M. Pelucchi, S. Arunthanayothin, Y. Song, et al., Pyrolysis and combustion chemistry of pyrrole, a reference component for bio-oil surrogates: jet-stirred reactor experiments and kinetic modeling, Energy Fuels 35 (9) (2021) 7265–7284.
[13] B. Lundberg, B. Sundqvist, O. Inganäs, et al., Pressure dependent electrical conductivity of polypyrrole, Mol. Cryst. Liq. Cryst. 118 (1) (1985) 155–158.
[14] H. Wahyudiono, S. Watanabe, Machmudah, et al., Pyrrole conversion induced pulse discharge plasma over a water surface under high-pressure argon, Chem. Eng. Process 61 (2012) 51–57.
[15] R. Goddard, O. Heinemann, C. Krüger, Pyrrole and a cocrystal of 1H- and 2H-1,2,3-triazole, Acta Crystallogr. C 53 (1997) 1846–1850.
[16] A. Lautie, F. Romain, Vibrational study of crystal phase transitions in pyrrole (C_4H_5N) and C_4D_5N, J. Raman Spectrosc. 21 (1990) 453–457.
[17] W.B. Li, D.F. Duan, X.L. Huang, et al., Pressure-induced diversity of π-stacking motifs and amorphous polymerization in pyrrole, J. Phys. Chem. C 118 (23) (2014) 12420–12427.
[18] P. Pruzan, Pressure effects on the hydrogen bond in ice up to 80 GPa, J. Mol. Struct. 322 (1994) 279–286.
[19] H. Wang, X. Li, G.Y. Gao, et al., Hydrogen-rich superconductors at high pressures, Wires Comput. Mol. Sci. 8 (1) (2018) e1330.
[20] M. Bauer, M.S. Elsaesser, K. Winkel, et al., Compression-rate dependence of the phase transition from hexagonal ice to ice II and/or ice III, Phys. Rev. B 7 (22) (2008) 220105.
[21] M. Fisch, A. Lanza, E. Boldyreva, et al., Kinetic control of high-pressure solid-State phase transitions: a case study on L-serine, J. Phys. Chem. C 119 (2015) 18611–18617.
[22] J. Ridout, L.S. Price, J.A.K. Howard, et al., Polymorphism arising from differing rates of compression of liquids, Cryst. Growth Des. 14 (2014) 3384–3391.
[23] Z.X. Du, K.Y. Shi, J.Q. Zhang, et al., Pressure-induced polymerization of crystalline and amorphous 3-nitrophenylacetylene, J. Phys. Chem. C 128 (6) (2024) 2418–2425.
[24] L. Zhang, K.Y. Shi, Y.L. Wang, et al., Compression rate-dependent crystallization of pyridine, J. Phys. Chem. C 125 (12) (2021) 6983–6989.
[25] K.K. Chu, C.S. Yuan, H.N. Li, et al., Pressure-induced amorphization and crystallization of choline chloride/ethylene glycol deep eutectic solvent, J. Mol. Liq. 242 (2017) 109–114.
[26] J. Wang, Q.Q. Yang, C.S. Yuan, et al., Dynamic pressure-induced amorphous transition and crystallization behavior of 4-methylpyridine, J. Mol. Struct. 1316 (2024) 138996.
[27] G.J. Piermarini, S. Block, J.D. Barnett, et al., Calibration of the pressure dependence of the R1 ruby fluorescence line to 195 kbar, J. Appl. Phys. 46 (6) (1975) 2774–2780.
[28] C.S. Yuan, X. Zhang, L.J. Zhou, et al., Phase transitions of carbon tetrachloride under static and dynamic pressures, J. Mol. Liq. 328 (2021) 115444.
[29] A.F. Goncharov, M.R. Manaa, J.M. Zaug, et al., Polymerization of formic acid under high pressure, Phys. Rev. Lett. 94 (2005) 065505.
[30] G. Liu, Gong J, L.P. Kong, et al., Isothermal pressure-derived metastable states in 2D hybrid perovskites showing enduring bandgap narrowing, Proc. Natl. Acad. Sci. USA 115 (2018) 8076–8081.
[31] Z.Y. Li, J. Gong, Z.K. Zhu, et al., Retention of high-pressure solutionprocessable metastable phase to ambience via differential sublattice rigidity for broadband photodetectors, Nat. Commun. 16 (2025) 2246.
[32] W.J. Evans, C.S. Yoo, G.W. Lee, et al., Dynamic diamond anvil cell (dDAC): a novel device for studying the dynamic-pressure properties of materials, Rev. Sci. Instrum. 78 (7) (2007) 073904.
[33] C. Suryanarayana, Phase formation under non-equilibrium processing conditions: rapid solidification processing and mechanical alloying, J. Mater. Sci. 53 (19) (2018) 13364–13379.
[34] P.C. Myint, J.L. Belof, Rapid freezing of water under dynamic compression, J. Phys.: Condensed Matter 30 (23) (2018) 233002.